J Electroceram (2008) 20:271–276
DOI 10.1007/s10832-007-9192-5

Investigation of omnidirectional piezoelectric actuator

P. Vasiljev · S. Borodinas · L. Vasiljeva · D. Mazeika · Seok-Jin Yoon

Received: 27 November 2006 / Accepted: 3 July 2007 / Published online: 18 July 2007

Abstract A study of a novel design composite piezoelectric actuator for omnidirectional object positioning is given in the paper. The actuator consists of a vibrating disc with a small cylinder mounted at the centre and a piezoceramic disc. The cylinder magnifies resonant bending vibrations of the vibrating disc and transmits driving force to the slider. Electrodes of the piezoceramic disc cover all the surface of the bottom and are divided into four equal sectors. 2D motion and rotation of the slider is achieved depending on the excitation scheme of the electrodes. Numerical modeling based on the finite element method was performed to obtain resonance frequencies and modal shapes of the actuator and to calculate the trajectories of contact point's movements under different excitation schemes of the electrodes. A prototype actuator was made and experimental outcomes of the oscillations of the working surfaces are given. Results of the numerical and experimental investigations are analyzed and discussed.

Keywords Piezoelectric actuator · Omnidirectional · Finite element method

P. Vasiljev · S. Borodinas · L. Vasiljeva
Department of Technical Subjects,
Vilnius Pedagogical University,
Studentu 39, Vilnius LT-08106, Lithuania

D. Mazeika (✉)
Department of Information Technology,
Vilnius Gediminas Technical University,
Vilnius LT-10223, Lithuania
e-mail: Dalius.Mazeika@fm.vtu.lt

S.-J. Yoon
Korea Institute of Science and Technology,
P.O. Box Cheongryang, Seoul 130-650, South Korea

1 Introduction

Piezoelectric actuators are widely used in the various technical systems such as high precision positioning devices, manipulators, micro robots, optical devices, etc [1, 2]. Specific characteristics such as compact size, high resolution and short response time, self-braking and absent of magnetic field make piezoelectric actuators attractive for actuation purposes in many mechanisms [1–4]. However, most of piezoelectric actuators are single degree of freedom devices and only few of them can achieve two-dimensional (2D) or multi-degree of freedom (MDOF) motion of the slider [5, 6]. Usually, mechanical systems composing several actuators are used for 2D or MDOF piezoelectric motors. It means that each degree of freedom uses separate actuator. Accuracy of the slider motion reduces applying this design principle to mechanical system. Obviously, the best way is to use only one actuator that can move or rotate the slider in any direction.

Operating principle of the MDOF actuators usually is based on combining two or more resonant modes of the actuator [5, 6]. Design of the actuator must be optimized, by minimizing difference between resonant frequencies of the combined modes if aforementioned operating principle is used. Otherwise amplitudes of the vibrations will be incomparable small.

A novel design of a MDOF piezoelectric actuator is proposed and analyzed in this paper. The actuator is named as omnidirectional because it can produce motion of slider in any direction in the plane. Operating principle of this actuator is based on using particular resonant mode that provides elliptical motion of the contact point. The advantage of this principle compare to others is the large vibration amplitudes [7]. Finite element modeling of the actuator was performed and an experimental prototype was made. This

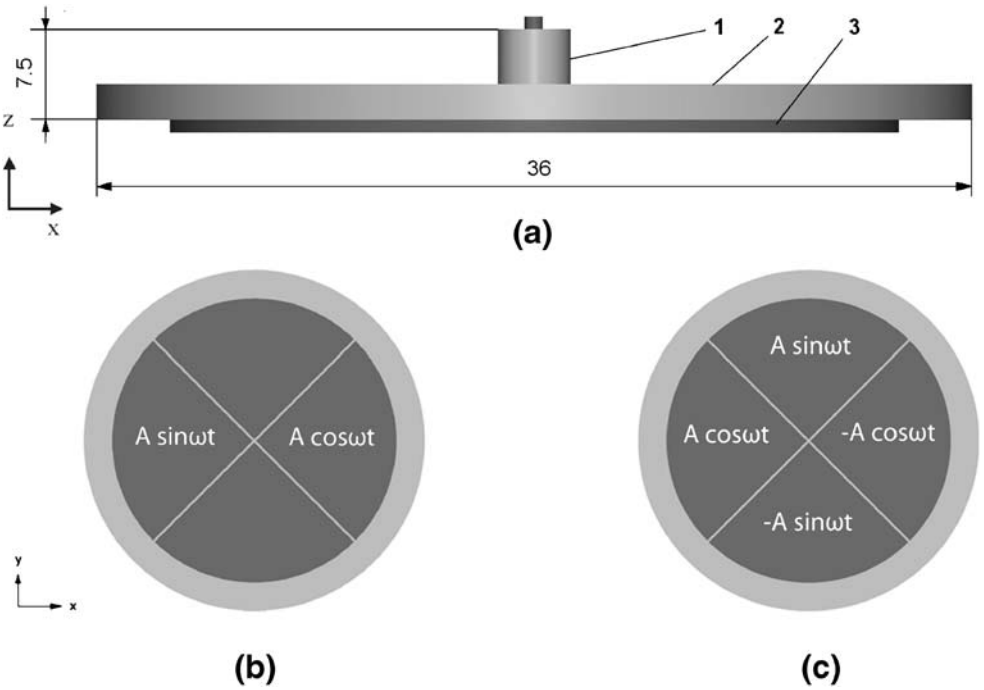

Fig. 1 (**a**) Schematic piezoelectric actuator: *1* cylinder with driving tip, *2* vibrating disc, *3* piezoceramic disc; excitation scheme for slider movement parallel to *x*-axis (**b**) and for rotation about *z*-axis (**c**)

newly developed piezoelectric actuator can be successfully used in sophisticated positioning or manipulating systems.

2 Design and operating principle of the actuator

A configuration of the piezoelectric actuator includes the following parts: a vibrating disc with the small cylinder mounted at the disc centre and a piezoceramic disc (Fig. 1(a)). Driving tip is located on the top of the cylinder. Both discs are glued together using adhesive. Electrodes are located at the bottom area of the piezoceramic disc and are divided into four equal sectors. Polarization of piezoceramic is oriented along thickness of the disc and d_{31} effect is used for actuation.

An elliptic trajectory of the contact point motion is achieved combining two components of cylinder (Fig. 1(a)) motion that is swinging and motion perpendicular to the surface of the disc. This type of cylinder motion is achieved using $B_{21,}$ B_{23} bending modes of the vibrating disc, where first subscript number means number of nodal circles and second means nodal diameters. These oscillation modes can be achieved when a pair of two opposite electrodes is excited using sinusoidal voltage with the same frequency but different phases shifted by $\pi/2$ (Fig. 1(b)).

The configuration of electrodes allows using different excitation schemes and to obtain oscillation modes of the disc with nodal diameters rotated by different angle. The direction of a nodal diameter coincides with the direction of the main axis of the contact point's elliptical motion and shows the direction of the slider movement. Using this type of actuator it is possible to achieve an omnidirectional movement of the slider in the plane. Two excitation schemes are analyzed in the paper as shown in Fig. 1(b) and (c). These schemes are used for linear (Fig. 1(b)) and rotational (Fig. 1(c)) motions of the slider.

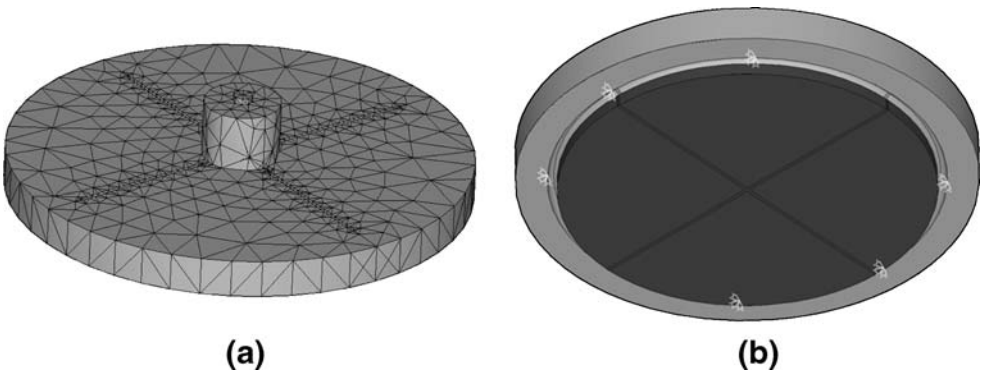

Fig. 2 Finite element model of actuator: (**a**) top view (**b**) bottom view

Table 1 Properties of the actuator materials.

Material properties	Piezoceramic PZT-8	Bronze
Young's modulus [N/m^2]	8.5×10^{10}	1.15×10^{11}
Poison's ratio		0.307
Density (kg/m^3)	7,600	8,760
Permitivity$\times10^{-9}$(F/m)	ε_{11}=11.42; ε_{33}=8.85	
Piezoelectric matrix (C/m^2)	e_{13}=−18.01; e_{33}=29.48; e_{52}=10.34	
Elasticity matrix,$\times10^{10}$ (N/m^2)	c_{11}=14.68; c_{12}=8.108; c_{13}=8.105; c_{33}=13.17; c_{44}=3.29; c_{66}=3.14	

3 FEM equations for actuator modeling

The finite element method (FEM) was used to perform modal frequency, harmonic response analysis, to calculate trajectories of the driven tip and to find admittance dependence on the frequency of input voltage. Basic dynamic equations of the piezoelectric actuator are derived from the principle of minimum potential energy by means of variational functionals and can be written as follows [8–11]:

$$\begin{cases} \mathbf{M}\ddot{u} + \mathbf{C}\dot{u} + \mathbf{K}u + \mathbf{T}\varphi = F, \\ \mathbf{T}^{\mathrm{T}}u - \mathbf{S}\varphi = \mathbf{Q}, \end{cases} \tag{1}$$

where **M**, **K**, **T**, **S**, **C** are matrices of mass, stiffness, electroelasticity, capacity and damping, respectively; $\boldsymbol{u}$, φ, $\boldsymbol{F}$, $\boldsymbol{Q}$ are, respectively, vectors of nodal displacements, potentials, external mechanical forces and charges coupled on the electrodes.

The driving force of the actuator is obtained from the piezoceramic disc. Finite elements discreetisation of the disc consists of elements with the nodes coupled with electrodes that have the known values of electric potential. The nodal electric potentials of remaining elements are calculated during solution. The dynamic equation of the piezoelectric actuator in this case can be expressed as follows [7, 8]:

$$\begin{cases} \mathbf{M}\ddot{u} + \mathbf{C}\dot{u} + \mathbf{K}u + \mathbf{T}_1\varphi_1 + \mathbf{T}_2\varphi_2 = \mathbf{F}, \\ \mathbf{T}_1^{\mathrm{T}}u - \mathbf{S}_{11}\varphi_1 - \mathbf{S}_{12}\varphi_2 = \mathbf{Q}_1, \\ \mathbf{T}_2^{\mathrm{T}}u - \mathbf{S}_{12}^{\mathrm{T}}\varphi_1 - \mathbf{S}_{22}\varphi_2 = \mathbf{0}, \end{cases} \tag{2}$$

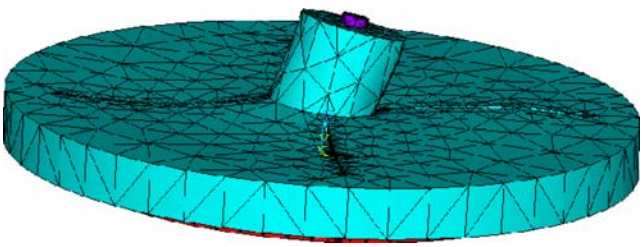

Fig. 3 Modal shape of actuator at 60.99 kHz

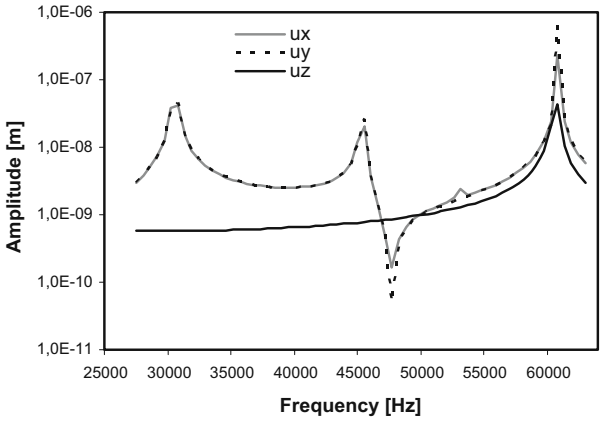

(a)

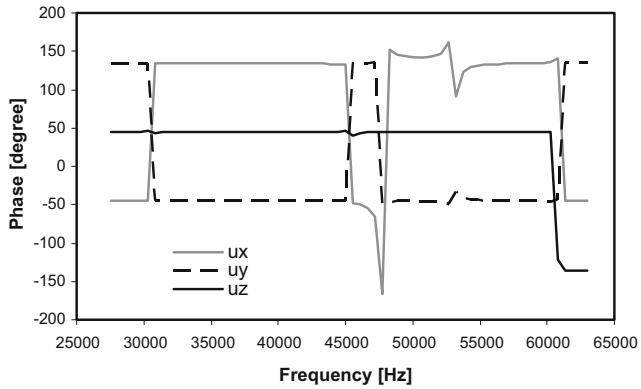

(b)

Fig. 4 Results of harmonic response analysis: (**a**) contact point's oscillation amplitude versus frequency; (**b**) contact point's oscillation phase versus frequency

here

$$\mathbf{T} = [\,\mathbf{T}_1 \quad \mathbf{T}_2\,], \mathbf{S} = \begin{bmatrix} \mathbf{S}_{11} & \mathbf{S}_{12} \\ \mathbf{S}_{12}^{\mathrm{T}} & \mathbf{S}_{22} \end{bmatrix}, \tag{3}$$

where φ_1, φ_2 are, respectively, the vector of nodal potentials of nodes coupled with electrodes and the vector of nodal potentials calculated during numerical simulation.

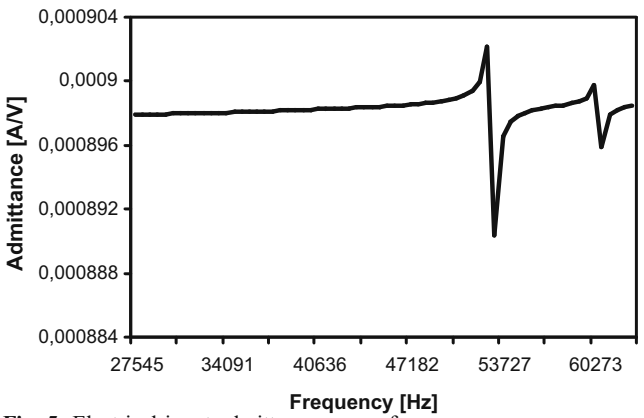

Fig. 5 Electrical input admittance versus frequency

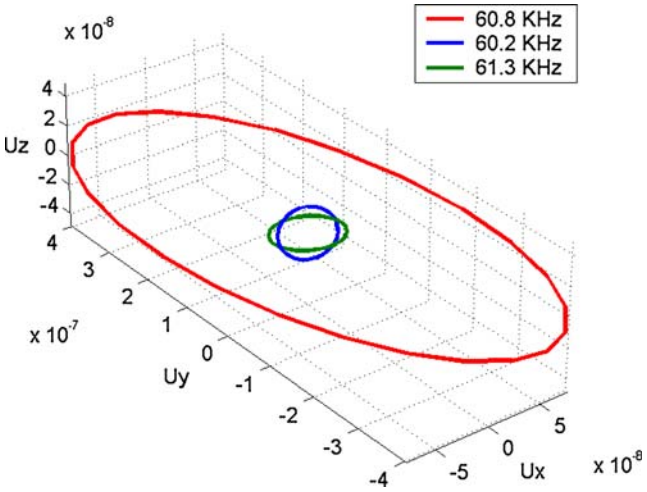

Fig. 6 Trajectories of contact point's movements for linear motion of slider in *xy* plane

Mechanical and electrical boundary conditions are determined for the piezoelectric actuator, i. e. mechanical displacements and velocities of the fixed surfaces of the actuator are equal to zero and the electric potential of the nodes that are not coupled with electrodes are equal to zero as well.

Natural frequencies and modal shapes of the actuator are derived from the modal solution of the piezoelectric system:

$$\det\left(\mathbf{K}^{*}-\omega^{2}\mathbf{M}\right)=0, \tag{4}$$

where **K*** is a modified stiffness matrix. In case when $\mathbf{Q}_1=0$ it can be written as follows:

$$\mathbf{K}^{*}=\mathbf{K}+\mathbf{T}\,\mathbf{S}^{-1}\mathbf{T}^{\mathrm{T}}. \tag{5}$$

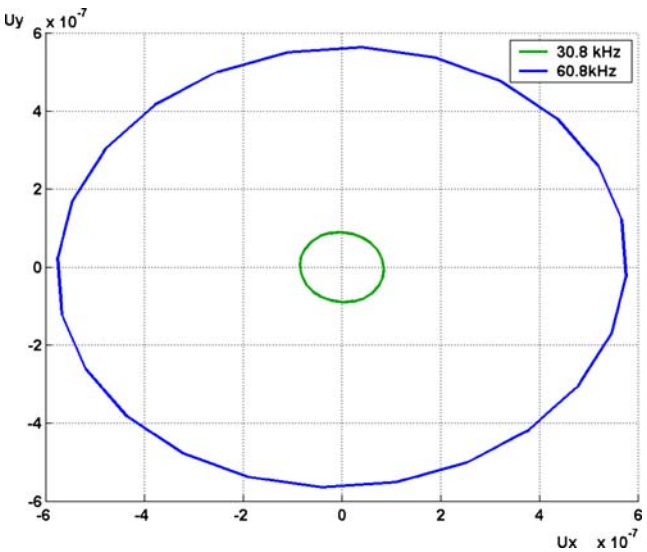

Fig. 7 Trajectories of contact point's movements when slider is rotating about *z*-axis

Table 2 Parameters of ellipses.

Excitation frequency (kHz)	Major axis (μm)	Minor axis (μm)	Ratio	Area (m^2)
Linear motion				
60.8	0.82085	0.11122	7.38	7.1707×10^{-14}
Rotation				
60.8	1.12511	1.1603	0.96	1.0253×10^{-12}

In the case when $\varphi_1=1$ the modified stiffness matrix is:

$$\mathbf{K}^{*}=\mathbf{K}+\mathbf{T}_2\,\mathbf{S}_{22}^{-1}\mathbf{T}_2^{\mathrm{T}}. \tag{6}$$

Harmonic response analysis is carried out applying sinusoidal varying voltage with different phases on electrodes of piezoelectric actuator. Due to the inverse piezoelectric effect corresponding mechanical forces are obtained:

$$\mathbf{F}_1=-T\varphi_1, \tag{7}$$

here a vector of nodal potentials φ_1 can be written as:

$$\varphi_1=\mathbf{U}\sin(\omega_{\mathrm{k}}t), \tag{8}$$

where $\boldsymbol{U}$ is a vector of voltage amplitudes, applied to the nodes coupled with electrodes. Referring to Eqs. 2, 7 and 8, the vector of mechanical forces can be calculated as follows:

$$\mathbf{F}_1=\left(\mathbf{T}_2\,\mathbf{S}_{22}^{-1}\,\mathbf{S}_{12}^{\mathrm{T}}-\mathbf{T}_1\right)\mathbf{U}\,\sin\left(\omega_k t\right). \tag{9}$$

Referring to Eq. 2 the vector of nodal charges $\boldsymbol{Q}_1$ can be written as follows:

$$\boldsymbol{Q}_1=\left(\mathbf{T}_1^{\mathrm{T}}-\mathbf{S}_{12}\,\mathbf{S}_{22}^{-1}\mathbf{T}_2^{\mathrm{T}}\right)u+\left(\mathbf{S}_{12}\,\mathbf{S}_{22}^{-1}\,\mathbf{S}_{12}^{\mathrm{T}}-\mathbf{S}_{12}^{\mathrm{T}}\right)\varphi_1. \tag{10}$$

Fig. 8 Prototype actuator

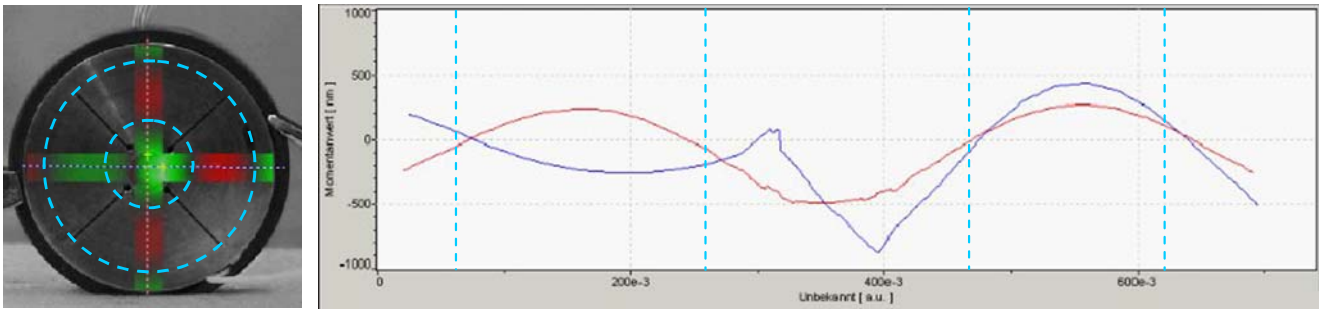

Fig. 9 Distribution of displacement amplitudes on the top surface of actuator at 57.9 kHz: (**a**) top surface view; (**b**) at two perpendicular diameters of top surface

Results for structural displacements of the piezoelectric actuator obtained from harmonic response analysis are used to determine the trajectory of the contact point's movement. Admittance values on nodes of piezoceramic finite elements can be determined as the function of frequency:

$$Y_i = \frac{Q_i}{U_i}\omega\, e^{j\left(\psi_i+\frac{\pi}{2}\right)}, \tag{11}$$

where j refers to the imaginary number, ψ is the phase. Calculated admittance dependence from the excitation voltage frequency will be compared with the results of the experiment.

4 Numerical simulation of the actuator

Numerical modeling of the piezoelectric actuator was used to verify and validate its design and operating principles through the modal and harmonic response analysis. FEM package ANSYS was employed in modeling and simulations. The finite element model consists of vibrating disc with the small cylinder and piezoceramic disc (Fig. 2). Adhesive layer is not used in the model. The model was built using 20-node structural solid brick elements SOLID95 and ten-node tetrahedral coupled-field solid elements SOLID98. SOLID95 elements were used to mesh the vibrating disc; the piezoceramic disc was meshed with SOLID98 elements.

Properties of the materials used for the actuator are listed in Table 1. Bronze was used for the vibrating disc, PZT-8 for the piezoceramic disc. An edge ring area at the bottom of the actuator was mechanically constrained in all directions (Fig. 2(b)).

Modal analysis of the piezoelectric actuator was done applying Block Lanczos eigenvalue solver. Damping was neglected in the FEM model. Analyzing results from modal analysis it was determined that mode B_{43} (60.99 kHz) can be used to move the slider (Fig. 3).

Harmonic response analysis was performed with the aims to find out the response of the actuator to the sinusoidal voltage applied on electrodes of the piezoceramic disc and to calculate trajectories of the contact point movement. Two excitation schemes were used in the simulations as shown in Fig. 1(b). Thirty volts AC signal was applied to electrodes. The movement of the slider towards the x coordinate axis and rotation about the z-axis can be achieved using these excitation schemes. The movement towards the y-axis was not simulated, because of the symmetry of the actuator.

A frequency range from 27 to 63 kHz with a solution at 545 Hz intervals were chosen and adequate response curves of contact point's oscillation amplitudes and phases were calculated. The contact point is located at the center of the top surface of the driving tip. Excitation scheme of the electrodes used for calculations is illustrated in Fig. 1(b). Results of calculations are given in Fig. 4(a) and (b) where the contact point's amplitude and phase versus frequency is given. Graphs of contact point oscillation amplitudes show that the excitation frequency at 30.8, 45.5 and 60.8 kHz has local peaks. Largest vibration amplitudes are at 60.8 kHz, therefore this frequency was chosen as the input frequency of the piezoelectric actuator for calculations of contact point trajectories.

Electrical input admittance over a frequency range 27–63 kHz was calculated. Results of the calculations are shown in Fig. 5. The admittance graph has two peaks. The first one shows B_{02} mode and the second B_{43} mode. Admittance graph confirms that piezoelectric actuator excitation frequency for trajectories calculation at 60.8 kHz was selected rightly.

Calculations of the contact point moving trajectories were done applying two excitation cases of the electrodes as shown in Fig. 1(b) and (c). Three different input voltage frequencies, i.e. 60.2, 60.8 and 61.3 kHz were used to simulate the motion of the contact point. It allows to compare parameters of trajectories and to show their strong dependency on the excitation frequency. Figures 6 and 7 illustrate trajectories of the contact point movement under excitation schemes shown in Fig. 1(b) and (c), respectively. It can be seen that trajectories have ellipsoidal shapes. Parameters of the ellipses are given in Table 2. Major axes of ellipses are rotated about

the centre of the coordinate system by the different angles and depend on excitation frequencies of the actuator (Fig. 6).

Contact point trajectories used for rotation of the slider are illustrated in Fig. 7. Actuator response at resonant frequencies 30.8 and 60.8 kHz were calculated for comparison. These trajectories are ellipsis and deflection of contact point motion at 60.8 kHz is much higher than at 30.8 kHz. Numerical simulations of the piezoelectric actuator have shown that small changes of the electric input signal frequency significantly influence the characteristics of the contact point movement.

5 Experimental investigation

A prototype actuator made for experimental investigation is shown in Fig. 8. The aims of this experiment were to verify resonant frequencies and trajectories of the driven tip movement that were calculated numerically and to find a distribution of the oscillation amplitudes on the top surface of the actuator.

Amplitude-frequency characteristics of the actuator were determined with the help of the 4192A LF impedance analyzer (Hewlett Packard). Oscillations of the top surface were measured using a laser Doppler vibrometer (POLYTEC CLV 3D). Resonant frequency at 57.91 kHz was determined analyzing electrical impedance of piezoelectric actuator. The difference between experimental and numerical resonant frequencies is 4.75%.

Measurements of the actuator top surface oscillations were done using two excitation schemes of electrodes as shown in Fig. 1(b) and (c). Results of measurements are given in Fig. 9. They confirm results of numerical modelling that the elliptical trajectory of the contact point can be achieved using this actuator. The distribution of oscillation amplitudes on the top surface of the actuator is same as was obtained in numerical simulations. The difference between the contact point's oscillation amplitudes obtained in numerical modelling and measured in experiments is 5–8%.

6 Conclusions

A MDOF piezoelectric actuator of the novel design was developed for an omnidirectional movement of the slider. Numerical and experimental studies validate suggested design of actuator and confirm the possibility to achieve elliptical trajectories of the contact point using different excitation schemes of the piezoelectric actuator. Values of the resonant frequencies and amplitudes from the finite element model are in good agreement with experimental results. Developed actuator has possibilities to move slider in any direction in the plane and rotate as well.

References

1. K. Uchino, *Piezoelectric Actuators and Ultrasonic Motors* (Kluwer, Norwell, MA, USA, 1997)
2. S. Ueha, Y. Tomikawa, M. Kurosawa, N. Nakamura, *Ultrasonic Motors: Theory and Applications* (Oxford University Press, USA, 1994)
3. G. Gautschi, *Piezoelectric Sensorics* (Springer, Berlin, Germany, 2002)
4. T. Hemsel, J. Wallaschek, Survey of the present state of the art of piezoelectric linear motors, Ultrasonics **38**, 37–40 (2000)
5. M. Aoyagi, S.P. Beeby, N.M. White, A novel multi-degree-of-freedom thick-film ultrasonic motor, IEEE Trans. Ultrason. Ferroelectr. Freq. Control **49**(2), 151–158 (2002)
6. Y.Gouda, K.Nakamura, S.Ueha, A miniaturization of the multi-degree-of-freedom ultrasonic actuator using a small cylinder fixed on a substrate. Proceedings of the 2nd International Workshop on Piezoelectric Materials and Applications in Actuators (Paderborn, Germany, 2005), pp. 263–267
7. T. Takano, Y. Tomikawa, M. Aoyagi, S. Hirose, Powder-supply device using bending mode disk vibrator with cylindrical funnel at its center, Proceedings of IEEE International Ultrasonic Symposium (Munich, Germany, 2002), pp. 657–660
8. H. Allik, T.J. Hughes, Finite element method for piezoelectric vibration, Int J Numer Methods Eng **2**, 151–157 (1970)
9. P.A. Juang, D.W. Gu, Finite element simulation for a new disc-type ultrasonic stator, IEEE Trans. Ultrason. Ferroelectr. Freq. Control **50**(4), 368–375 (2003)
10. H.S. Tzou, *Piezoelectric Shells Distributed Sensing and Control of Continua* (Kluwer, Dordrecht, 1993) p. 320
11. P. Vasiljev, S. Borodinas, S.-J. Yoon, D. Mazeika, G. Kulvietis, The actuator for micro moving of a body in a plane, Mater. Chem. Phys. **91**(1), 237–242 (2005)